Magnetically recyclable core–shell structured Co$_{0.5}$Zn$_{0.5}$Fe$_2$O$_4$@polyaniline nanocomposite: high stability and rapid photocatalytic degradation of commercial azo dyes and industrial effluents

Md. Rigan Islam Riyat[1] · Abdus Salam[2] · Md. Tamzid Hossain Molla[1] · Md. Suman Islam[1] · Md. Abul Bashar[1] · Dipesh Chandra[1] · Shameem Ahsan[3] · Debashish Roy[4] · Md. Shameem Ahsan[1]

Abstract

A nanocomposite photocatalyst, Cobalt-Zinc-Ferrite @Polyaniline (CZF@PANI) was synthesized via co-precipitation and in-situ oxidative polymerization methods, to treat commercial dyes and industrial effluents. The formation of the spinel ferrite structure of nanoparticles (CZF) and the core–shell structure of CZF@PANI were confirmed by spectral analyses. By using multi-point analysis, the BET surface area of the CZF@PANI photocatalyst was found to be 25.14 m^2/g. The photocatalytic performance of CZF@PANI was validated by the degradation mainly of reactive orange (RO-14) and dispersed red (DR-1) and exhibited superior degradation (> 99%). The activity of CZF@PANI was almost unchanged even after 25 cycles of degradation of RO-14. This indicates extremely high stability. Furthermore, three more synthetic dyes, real textile and tannery wastewater samples were also subjected to treatment by CZF@PANI and showed considerable degradation. pH, BOD, and COD values were decreased to the Business for Social Responsibility (BSR) standard range in the tested textile wastewater sample. The composites' simple synthesis, high degradation capability, excellent stability and regenerability may provide a highly efficient and cost-effective photocatalyst for water remediation.

✉ Md. Shameem Ahsan
shameem@ru.ac.bd

[1] Department of Applied Chemistry and Chemical Engineering, University of Rajshahi, Rajshahi 6205, Bangladesh

[2] Chemical and Paper Engineering, Western Michigan University, 4601 Campus Drive, Kalamazoo, MI 49008-5462, USA

[3] Department of Chemistry, Govt. Zaheda Safir Mohila College, Jamalpur, Bangladesh

[4] Industrial Environment Management, Square Fashions Ltd, Dhaka, Bangladesh

Graphical abstract
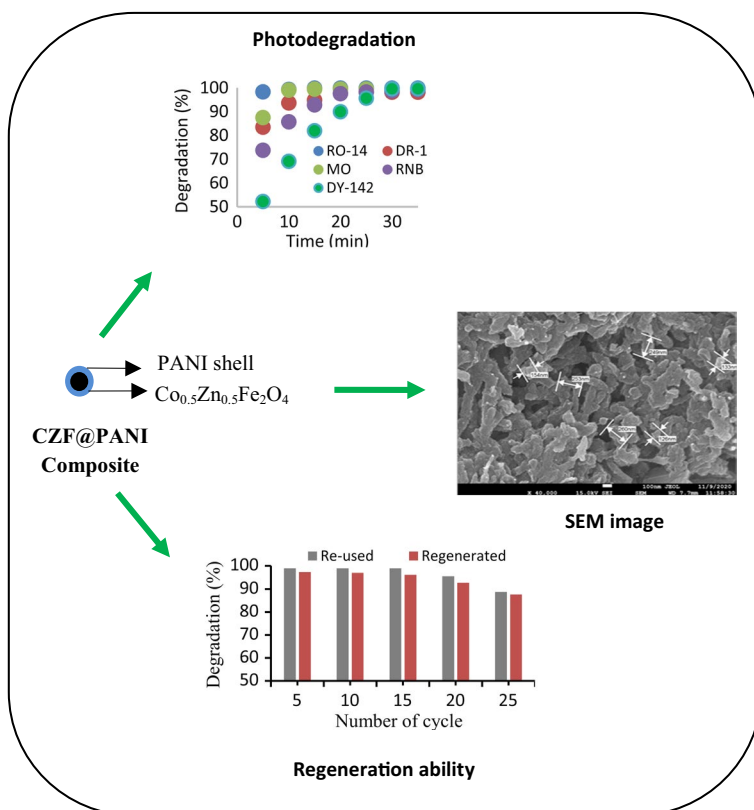
Introduction

Textile dyeing and wet processing operations are associated with the generation of toxic wastewater.They have high biological oxygen demand (BOD), chemical oxygen demand (COD), acidity, high suspended and dissolved solids, dyestuffs, heavy metals, and other soluble substances because various types of dyes are used to colour their products [1]. On the other hand, the chemicals used in leather tanning are not fully taken up by the hide/skins and thus, finish up in tannery wastewater, as a major source of well-documented environmental (soil/water) pollution and severe health threats in living beings [2]. Therefore, it is crucial to develop and implement innovative technologies for treating water at high efficiency with low energy consumption. The traditional photocatalysts (such as TiO_2, ZnO, and Bi-based oxide

semiconductors), with wide bandgaps, are active only in the ultraviolet (UV) region, and the rapid recombination rate of the photogenerated electrons and holes leads to a low quantum efficiency, which limits their practical application in wastewater treatment [3–6]. Therefore, there is a great interest in designs of catalysts for pollutant degradation without complicating light illumination. There is also interest in adding additional reagents with high reusability, like H_2O_2/O_3, into the Fenton process. However, the main technological barrier preventing the commercialization of photocatalysts is the post-recovery of the catalyst particles after the water treatment. Fortunately, magnetic separation is an effective technique to remove and recycle the photocatalysts from water by applying an external magnetic field [7]. Among the magnetic materials, spinel structures have attracted wide interest by virtue of their strong magnetic recyclability, visible light activity, chemical stability, low cost, nontoxicity and environment-friendliness. In magnetic separation, Co-Zn ferrites, represented by the formula $(Zn_A^{2+}Fe_A^{3+})[Co_B^{2+}Fe_B^{3+}]O_4^-$, all of the metallic ions Fe^{3+}/Zn^{2+} occupy the tetrahedral sites and the metallic ions Fe^{3+}/Co^{2+} occupy the octahedral sites [8]. The incorporation of active nano-material in a polymeric matrix is advantageous in the separation and transfer of photoinduced electrons (e^-) and holes (h^+), which can increase the photocatalytic activity and stability of the semiconductors. PANI is a kind of π-conjugated long-chain polymer and the protonic acid-doped PANI possesses very high conductivity. PANI has three redox states, among them the leucoemeraldine based-PANI possesses a weak reduction capability because of the existence of $-NH-$ bonds connecting the benzene rings [9]. The remarkable catalytic performance of semiconductor-PANI shows that PANI not only acts as a good electron donor from its LUMO orbital but is also as an excellent hole acceptor/conductor in HOMO orbital. After harvesting visible light, PANI substantially retards the recombination of light-induced charge-hole carriers [10]. Moreover, PANI has a simple and reversible acid/base doping/de-doping chemistry to achieve regeneration and enable reuse of such carriers. To the best of our knowledge, however, the study of the composite photocatalyst CZF@PANI has rarely been reported.

In the present study, a simple method is used to synthesize magnetically separable CZF@PANI composite. Its photocatalytic activity was measured against reactive orange (RO-14), disperse red (DR-1), reactive navy blue RX (RNB), direct yellow (DY-142), and methyl orange (MO) dyes, and also on real textile and tannery wastewaters. Specifically, the effects of pH, photocatalyst dosage, and the initial dye concentration were investigated in the degradation of reactive orange (RO-14) and disperse red (DR-1) dyes as model pollutants. The stability and reusability of the composite were checked for several RO-14 discoloration runs. Finally, a probable photocatalytic mechanism is discussed in detail.

Experimental section

Materials

All chemicals were of analytical grade and used without further purification. Sodium hydroxide pellets (NaOH), hydrochloric acid (HCl), aniline (ANI) and, absolute

ethanol were procured from Sigma-Aldrich. Anhydrous ferric chloride ($FeCl_3$), cobalt chloride hexahydrated ($CoCl_2 \cdot 6H_2O$), anhydrous zinc chloride ($ZnCl_2$), and ammonium persulfate [$(NH_4)_2S_2O_8$] were purchased from Merck Germany. Reactive orange-14 (RO-14), Disperse red-1 (DR-1), Reactive navy blue RX (RNB), Direct yellow-142 (DY-142) and Methyl orange (MO) were taken from Loba-Chemie Pvt Ltd. The real textile dyeing wastewater was collected from Square Textiles, Valuka, Bangladesh, and the tannery effluent was taken up from Apex Leather Industries, Savar, Bangladesh.

Synthesis of magnetic CZF nanoparticle

The magnetic CZF nanoparticle was prepared by the aqueous co-precipitation method under alkaline conditions using NaOH as a base. Cobalt chloride hexahydrated ($CoCl_2 \cdot 6H_2O$), zinc chloride ($ZnCl_2$) and ferric chloride ($FeCl_3$) with a molar ratio of 0.5:0.5:1 were dissolved separately in 100 mL of distilled water. The prepared solutions were mixed in an Erlenmeyer flask, placed in a water bath at room temperature with continuous stirring for 1 h, and sonicated for 30 min using an ultrasonic bath for good dispersion. 2 M NaOH was then added to the mixture solution dropwise as a precipitating agent, under constant stirring, to adjust different pH values (optimum pH 12.5). The reaction flask was covered to diminish the evaporation of the solution. The liquid residue was then brought to a reaction temperature of 80 °C for 3.5 h, under constant stirring, to transform hydroxides into spinel ferrite resulting in a black colour precipitate of nanoparticle. The synthesized nanoparticle was separated, washed several times with absolute ethanol and distilled water to remove the unreacted residual salts, and dried at 120 °C for 5 h in a hot air oven. Furthermore, the product was calcinated at 550 °C for 2 h in a muffle furnace, in order to improve the crystalline nature of the CZF nanoparticle.

Synthesis of CZF@PANI composite

Synthesis of CZF@PANI composite was conducted by in-situ oxidative polymerization of aniline with the CZF nanoparticle. At first, 5 g of CZF (heated for 1 h at 60 °C before adding) was dispersed in 1 M of HCl aqueous solution with simultaneous mechanical stirring for 30 min and ultrasonic vibrations for 30 min to activate the surface of CZF. At ratio 3:2 (mg/ml), CZF and aniline (refrigerated 60 min before adding) were added into a Erlenmeyer flask, and stirred for 30 min under ice bath conditions (below 5 °C). Ammonium persulfate (equimolar to aniline) was dissolved in 1 M HCl aqueous solution (refrigerated 30 min before adding) which was added dropwise to the above mixture and allowed to polymerize under stirring for 6 h in the ice bath below 5 °C. The mixed solution was then allowed to react for 12 h at room temperature without any disturbance. Finally, the filtered composite was washed with an excess amount of distilled water, and dried at 80 °C until a constant mass was obtained.

Characterization

The chemical nature of the CZF and CZF@PANI surfaces were analysed by Fourier Transform Infrared (FTIR) spectrophotometer-3000 Hyperion Microscope Vertex 80. The FTIR spectra were obtained from KBr-pressed pellets in the range 3800–400 cm^{-1} with 1 cm^{-1} resolution. The crystalline structure of the synthesized CZF and CZF@PANI composite were analyzed by powder X-ray Diffraction (XRD) using XPERT-PRO diffractometer system with Cu K_α radiation (λ = 1.54056 Å) at 45 kV and 35 mA, the data were collected at 295 K with a step-scan procedure from 25 to 70° (2θ) using a step size of 0.05° and 1.0 s per step. The morphology and size of the CZF nanoparticle and CZF@PANI composite were characterised by JEOL, JSM-7610F the Field Emission Scanning Electron Microscope (FESEM). The elemental constituents of the composite were determined by Energy-dispersive X-ray (EDX) spectroscopy that was integrated into the SEM system. An X-ray photoelectron spectrometer (XPS) system (VG Multilab 2000 Thermo Scientific, USA, K-Alpha) with a multi-channel detector capable of withstanding high photonic energies ranging from 0.1 to 3 keV was utilized to explore chemical composition, oxidation states, and binding energies of various atoms in the CZF@PANI photocatalyst. The Brunauer, Emmett, and Teller (BET) method was used to calculate BET specific surface areas from nitrogen adsorption–desorption isotherms measured by Belsorp mini II (BEL Japan Inc.) at 70 °C under vacuum for 5 h.The thermal properties were determined by Thermogravimetric (TG) analysis carried out using a Perkin Elmer Thermal Analyzer, at a heating rate of 10 °C/min from 20ºC to 800ºC in the air, having a flow rate of 20 mL/min. Finally, the UV–Vis absorption analysis was recorded by the HACH Spectrophotometer, over the wavelength range of 200–800 nm to identify the photocatalytic performance of CZF@PANI composite as photocatalyst.

Photocatalytic experiments

In this study, two azo dyes, RO-14 and DR-1, were used as model pollutants to study the photocatalytic performance of the CZF@PANI photocatalyst. In addition to real textile and tannery waste water, the degradant was also applied to more three reactive dyes such as RNB, DY-142, and MO. First, the CZF@PANI photocatalyst was activated at the optimum condition to increase the catalytic activity. In a typical batch test, 150 mL substrate solution and a certain amount of photocatalyst were fed into a glass beaker. A magnetic stirrer was used to continuously agitate the suspensions at a rate of 350 rpm for all the experimental runs. Before photocatalytic reaction, the heterogeneous mixture was pre-mixed in the dark for 20 min, so as to achieve adsorption–desorption equilibrium of pollutant on the catalyst surface. Next, the solution was exposed to halogen light irradiation as a visible light source. After specific time intervals, 4 mL of solution was withdrawn from the system and photocatalyst particles were separated, using a strong magnet, in a few seconds. Using a UV–Vis spectrophotometer, the amount of the

reduction in the concentrations of the dyes during photocatalytic experiment were recorded. The degradation efficiency was calculated using the following equation-

$$\text{Degradation efficiency} = \frac{C_0 - C_t}{C_0} \times 100 \tag{1}$$

here, C_0 is the initial concentration of dye and C_t is the final concentration of dye at reaction time, t (min).

Results and discussion

Characterization

FTIR analysis

The characteristic FTIR spectrum for CZF and CZF@PANI are shown in Fig. 1A. The bare magnetic nanoparticle exhibits a broad peak between 3437 cm^{-1}. This is due to the –OH stretch band which is associated with the lattice surface of ferrite at the time of sample preparation by co-precipitation method [11]. The band appears at 1636 cm^{-1} and is attributed to the stretching vibration of the hydrogen bonded O--H groups. The spectra consist of two main peaks, located at about 610–569 cm^{-1} and 480–460 cm^{-1}, which confirm the formation of a spinel ferrite structure [12]. The 589 cm^{-1} peak is due to vibration of the tetrahedral sublattice, while 465 cm^{-1} peak is due to vibration of the octahedral sublattice in the spinel structure. The characteristic FTIR spectrum of CZF@PANI clearly shows that main characteristic bands of 1565 cm^{-1} and 1474 cm^{-1} correspond to the quinonoid and benzenoid rings and unveil the presence of emeraldine form of PANI. The peaks at 1292 cm^{-1} and 1234 cm^{-1} can be attributed to the C--N bond stretching mode of the benzene ring. The very strong and wide peak at 1135 cm^{-1} is delineated as the electronic-like
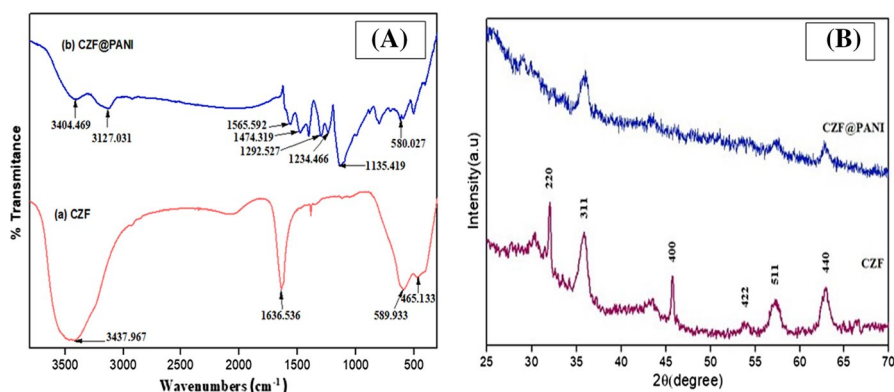

Fig. 1 **A** FTIR spectra of *a* CZF nanoparticles, and *b* CZF@PANI composite; **B** XRD patterns of CZF nanoparticle and CZF@PANI composite

band of the quinoid unit of doped PANI. However, the characteristic peaks of CZF@
PANI composite shift to a lower wave number as compared to pure PANI [13, 14].
This shift of the characteristic peaks can be attributed to the interaction between qui-
none and quinonoid nitrogen of PANI polymer chains and metal-oxide linkages of
CZF, which delocalise the electron density and bond energy of the PANI, after the
incorporation of CZF during in-situ polymerisation [15].

XRD analysis

The result obtained from the XRD pattern (Fig. 1B) of CZF with the (hkl) val-
ues corresponding to the diffraction peaks of different planes (220), (311), (400),
(422), (511) and (440) is either even or odd, indicating the sample is spinel cubic
structured [16]. The XRD pattern of the CZF@PANI revealed that the diffraction
peaks, which correspond to the polyaniline semicrystallinity disappeared. This was
due to the restricted polymer-chain alignment in the presence of the nanoparticle.
The crystalline peaks which correspond to CZF nanocrystal are focused at (311),
(422), (511) and (440) with reduced intensity due to polymer coating. This phenom-
enon originates from the coating effect of PANI on the surface of CZF. The surface
attachment of PANI to the CZF nanoparticle does not affect the spinel-type crystal
structure [13].

SEM and EDX analyses

The SEM image of CZF (Fig. 2A) shows a nearly-spherical rod-like structure.
This is produced by stacking tiny particles in an agglomerated form on top of one
another. The particle size of the CZF nanoparticle (between 84.1 and 90.1 nm) and
the observed agglomeration of the nanoparticle may be due to the magnetic interac-
tion among nanoparticles. Each nanoparticle acts as a magnet to the others [17].
SEM images of CZF@PANI, Fig. 2B reveal that all the particles were success-
fully coated with the PANI layer. The micrograph exhibited a core–shell-structured
CZF@PANI composite matrix, with size ranging from 126 to 260 nm. The bigger
particle sizes in the composite, compared to those in pure CZF, could be due to the
coating of PANI around the surface of the CZF nanoparticle.

The presence of elements O, Fe, Co, Zn in a pure CZF particle were confirmed by
EDX analysis (Fig. 2C). No trace of any impurity was found, indicating the purity
of the sample as prepared. As shown in Fig. 2D, CZF@PANI composite consists of
elements like C, N, O, Fe. Co, Zn etc. The presence of C and N peaks was evidence
of the benzenoid and quinoid groups in the polyaniline structure. The other elemen-
tal peaks may come from the reactant molecules (dopant-HCl and oxidant-APS).

Surface area of CZF@PANI photocatalyst

The BET surface area of the CZF@PANI photocatalyst was found to be 25.14 m^2/g
using multi-point analysis. The photocatalyst with greater surface area provides a
large number of sites to fix more dyes from wastewater. The pore volume and aver-
age pore diameter were identified as 6.02×10^{-2} cm^3/g and 9.57 nm. The skeletal
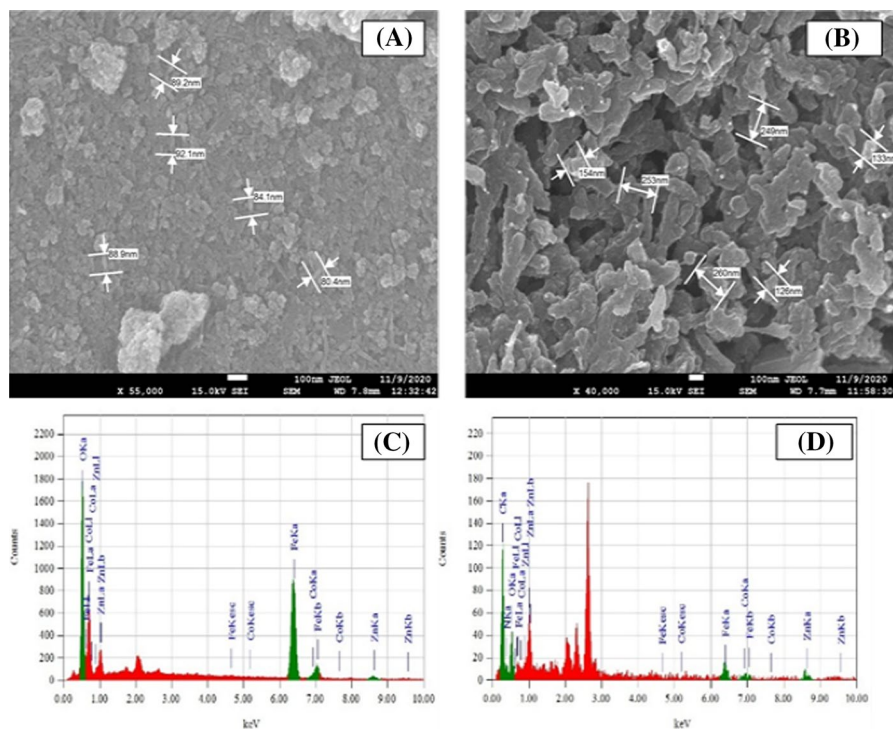
Fig. 2 SEM images of **A** CZF nanoparticle, and **B** CZF@PANI composite; EDX spectra of **C** CZF nanoparticle, and **D** CZF@PANI composite

density was measured to be 2.8526 g/cm^3 and the porosity was 0.1465 per gram of sample.

XPS analysis

X-ray photoelectron spectroscopy (XPS) was used to determine the chemical composition, oxidation states, and binding energies of various atoms in the CZF@PANI photocatalyst. The XPS survey spectra of the synthesized photocatalyst in the binding energy range of 0 to 1350 eV indicate the presence of Co, Zn, Fe, O, C, and N (Fig. 3a). The high-resolution XPS spectra of Co-2p, Zn-2p, Fe-2p, O-1s, C-1s, and N-1s are shown in Fig. 3.

It is observed from Fig. 3b that the Co-2p XPS spectrum exhibits two peaks at 795.08 eV and 780.58 eV, corresponding to the Co-2p$_{1/2}$ and Co-2p$_{3/2}$ spin orbits, respectively. The binding energies of Co-2p$_{1/2}$ at 794.48 and 796.58 eV are associated with the distribution of Co^{2+} ions in the tetrahedral and octahedral sites. The Zn-2p spectra show two peaks at 1021.28 eV and 1044.38 eV, associated with Zn 2p$_{3/2}$ and Zn 2p$_{1/2}$, respectively, indicating that Zn exists mainly in the + 2 oxidation state (Fig. 3c). The energy separation between these two peaks was measured at
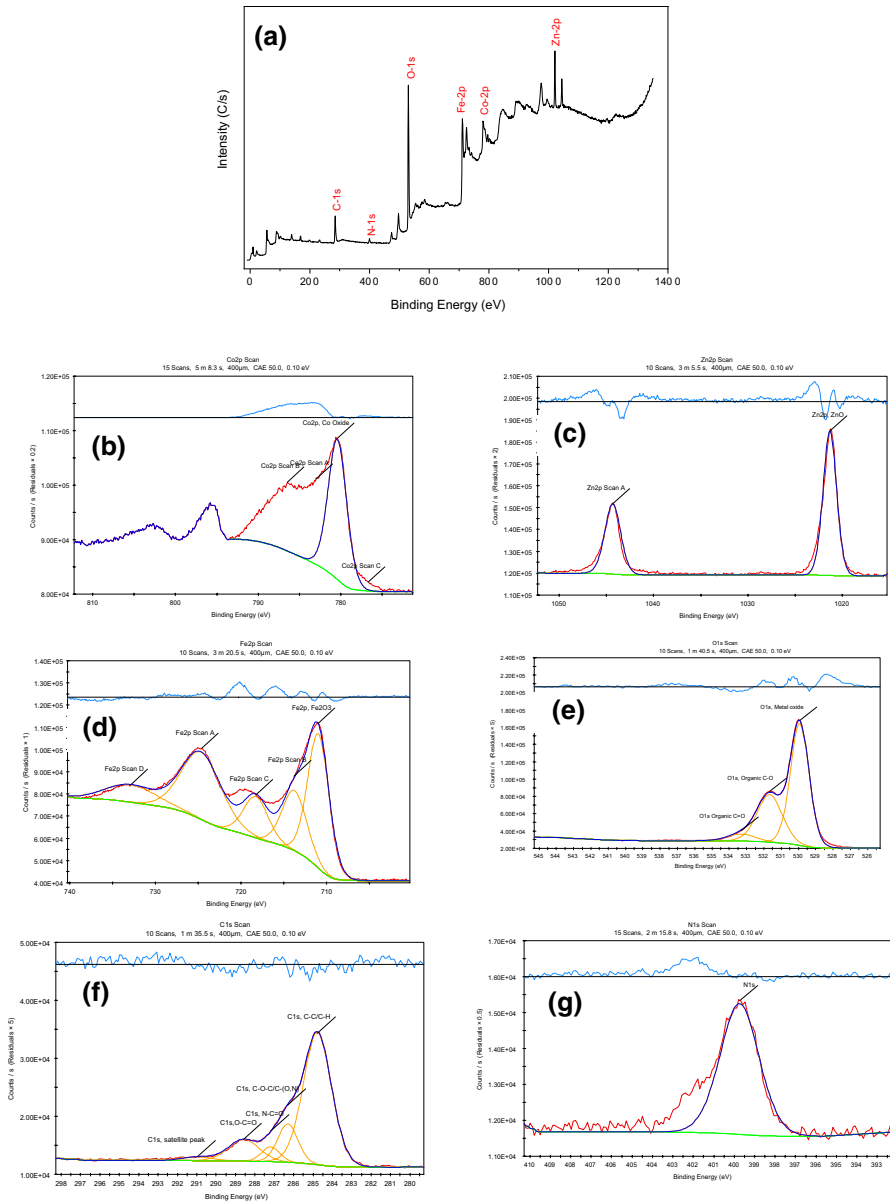
Fig. 3 XPS spectra of CZF@PANI photocatalyst **a** Survey scan from 0 to 1350 eV; Narrow scan for **b** Co-2p in the range of 770–805 eV **c** Zn-2p in the range of 1015–1052 eV **d** Fe-2p in the range of 700–740 eV, **e** O-1s in the range of 525–545 eV, **f** C-1s in the range of 280–298 eV **g** N-1s in the range of 392–410 eV

23.1 eV, which is a characteristic signal from the Zn^{2+} species. In Fig. 3d, two strong peaks were observed in the narrow XPS spectra of Fe-2p. The peak at 710.98 eV is due to Fe-$2p_{3/2}$ and the peak at 724.58 eV is due to Fe-$2p_{1/2}$, revealing that Fe exists

mainly in the + 3 oxidation state in the photocatalyst. The two peaks are disjointed with an energy value of 13.6 eV. Fig. 3e shows the spectra of O-1s. The peak at 529.98 eV is assigned to the contribution of crystal lattice oxygen; additionally, the peaks at 531.58 and 532.88 eV are ascribed to the organic oxygen, contaminants, chemisorbed and physisorbed water on the surface of the photocatalyst. Fig. 3f displays the deconvoluted C-1s spectrum of CZF@PANI, revealing the presence of three different types of carbon functional groups, namely, non-oxygenated carbon (C–C, CH) at 284.88 eV, oxygenated carbon (C–O–C, O–C=O) in the range of 288.58 eV, and nitrogenated carbon (N–C=O, C–N, C=N) near 286.28–287.08 eV. The N-1s spectrum (Fig. 3g) shows three peaks: 398.28 eV for the quinoid amine, 399.48 eV for the benzenoid amine, and 401.08 eV for the reduced nitrogen cationic radical (N^+). These findings imply that PANI was protonated in the ternary composite (CZF@PANI).

TG analysis

Fig. 4 is depicted the TGA curves of PANI, CZF and CZF@PANI hybrid composite. The weight loss of CZF in the range of 20 to 800 °C is about 10%. Due to the removal of adsorbed water, the weight loss in the low temperature region ($\leq$ 300 °C) is slightly greater, while the relatively smaller weight loss in the high temperature region may be attributed to a comperatively small amount of metal hydroxide decomposition. In the case of PANI, the initial weight loss occurs at around 85 °C because of water evaporation and the loss of doped HCl. The weight loss in the range of 150–536 °C most likely occured due to the volatilization of lower weight PANI or to the decomposition of PANI chains. As for CZF@PANI, the initial 9% weight loss in the range around 20–115 °C is due to expulsion of residual water molecules/solvents. During the second step, from 115 to 330 °C, thermal degradation of the low weight oligomers occurs. From 330 to 600 °C, the major weight loss of approximately 56% is due to the thermal degradation of the polymer formed. Finally, above 600 °C, approximately 65% of the composite, PANI, was burnt out, while 35% of the composite, CZF, remained as
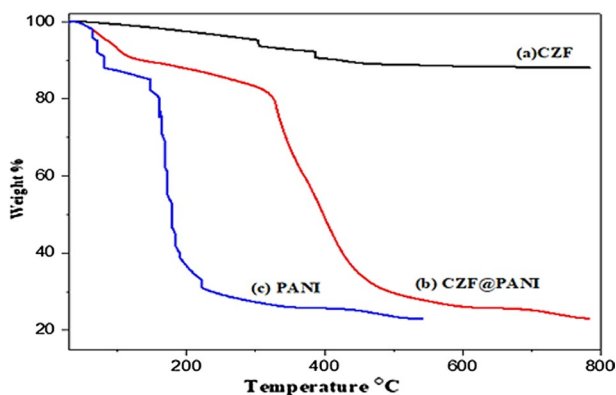

Fig. 4 TGA curves of *a* CZF, *b* CZF@PANI, and *c* PANI

residue. This implies that the 65% of the composite, PANI, were doped on to the surface of the CZF nanoparticles.

Influences of different synthesis parameters over photocatalytic activity

Influence of calcination temperature on CZF nanoparticle

Different temperatures within the range of 250 to 650 °C were applied for 2 h to investigate the influence of CZF calcination temperature on the photoactivity of the CZF@PANI composite. The results showed that increasing the calcination temperature enhances the photoactivity of the composite on RO-14 and DR-1 dye degradation process and the maximum activity was achieved at 550 °C. At 550 °C, complete burning occured, and the presence of CZF in the sample reached a maximum value. A calcination temperature over 550 °C would risk an adverse effect on the catalytic performance of CZF@PANI composite. The deterioration of photocatalytic efficiency is attributed to particle segregation of CZF after calcination at higher temperatures [18].

The optimum PANI content in CZF@PANI composite

At a lower molar ratio of CZF and aniline (g/ml), the adsorption and photocatalytic activity of PANI decreases because active sites become limited. Excess PANI would cause overlapping agglomerates and hinder the direct contact of the CZF surface with the dyes, resulting in less photocatalytic degradation of RO-14 and DR-1 dyes. The optimum molar ratio of CZF and aniline at 1:0.67 produced the greatest photocatalytic degradation. In contrast, the appropriate PANI content caused a uniform dispersion on the CZF surface, which was beneficial to the transfer and separation of the electrons and holes.

Effect of pH in the formation of CZF

In CZF nanoparticle formation, the concentration of NaOH in the reaction system was chosen to be 2 M to maintain the pH 10 and pH 12.5, and the reaction temperature was 80 °C. At pH 10, the yield of CZF nanoparticle formation was 50.63% and at pH 12.5, it was 74.27%. There was a remarkable increase in nanoparticle formation when the solution pH was increased from 10 to 12.5. The concentration of NaOH had a significant role on the nucleation rate. High concentration of OH^- could lead to lower nuclei concentration of Co^{2+}, Zn^{2+} and Fe^{3+}. When the pH of the reaction system increases, $Co(OH)_2$, $Zn(OH)_2$ and $Fe(OH)_3$ are generated in the first step. This occurs because of the hydrolysis of Co^{2+}, Zn^{2+} and Fe^{3+}, and the formation of the nanoparticle.

Effect of HCl concentration in polymerization process

A prominent difference in degradation capability was observed in the composite, when the polymerization of aniline on CZF surface was done by different concentrations of acid medium. A series of experiments were carried out to study the effect of

acid concentration on the formulation of the PANI layer on the CZF surface. When complete polymerization occured on the CZF surface, PANI absorbed its highest amount of pollutants and visible light, and showed the highest photocatalytic activity. The concentrations of dopant (HCl) were selected to be 0.1 M, 0.3 M, 0.5 M, 0.7 M, 1.0 M, 1.5 M, and 2.0 M. The increasing HCl concentration in polymerization of aniline on the CZF surface increased the photocatalytic activity of the CZF@PANI composite. When HCl concentration increased above 1.0 M, there was no change in photocatalytic activity.

Influence of different parameters on photocatalytic degradation of RO-14 and DR-1

Effect of photocatalyst loading

Effects of catalyst dosage on the degradation of RO-14 and DR-1 were observed by adding 0.5, 1.0 and 1.5 g/L of CZF@PANI catalyst in the reactor to 150 mL of RO-14 and DR-1 solutions at pH 7.0 with the initial dye concentration of 30.0 mg/L. Fig. 5a and b show that the degradation rate increases with an increase in catalytic dosage, this is a characteristic of heterogenous photocatalysis [19]. With the increase in catalyst dosage, the available active sites on the catalyst surface responsible for the generation of hydroxyl radical (OH˙) increases. As a result, the rate of degradation also increased. The half-life of the intermediates decreased with increasing catalyst dosage, which implied that the intermediates were degraded very fast. In turn this implies the mineralization of the dye molecules [20]. However, increasing the catalyst loading beyond a certain amount can lead to lower degradation efficiency because of the light-scattering effect and an increase in the particle aggregation [21]. For this reason, using 1.5 g/L of photocatalyst showed the nearly same result as using 1 g/L photocatalyst.

Effect of pH

Degradations of RO-14 and DR-1 by CZF@PANI composite were investigated at pH 3, 5, 7, 9 and 11 (Fig. 5c, d). It was found that either in basic (pH 9, 11) or acidic (pH 3, 5) conditions, CZF@PANI displayed nearly the same degradation efficiency as in neutral conditions (pH 7) and the efficiency reached as high as nearly 100% over the entire pH range (3–11). In basic conditions, the pH gradually decreased and reached a steady state at near neutral, while in acidic conditions, the initial pH gradually increased. The starting solution, with a high pH, contains more OH^- anions, which could act as hole (h^+) scavengers and react with photogenerated h^+ to form active OH˙ radicals. Hence, the consumption of OH^- led to a decrease in pH over the reaction time. The OH˙ radicals have a strong oxidation ability to degrade pollutants. On the other hand, the starting solution with a low pH contains more H^+ ions, which can serve as electron scavengers, and inhibits the recombination of e^-–h^+ pairs. Moreover, the H^+ reacts with $O_2^{˙-}$ to form hydrogen peroxide, that decomposed into oxidative OH˙ under visible light irradiation (Eq. 7). Thus, the suppressed
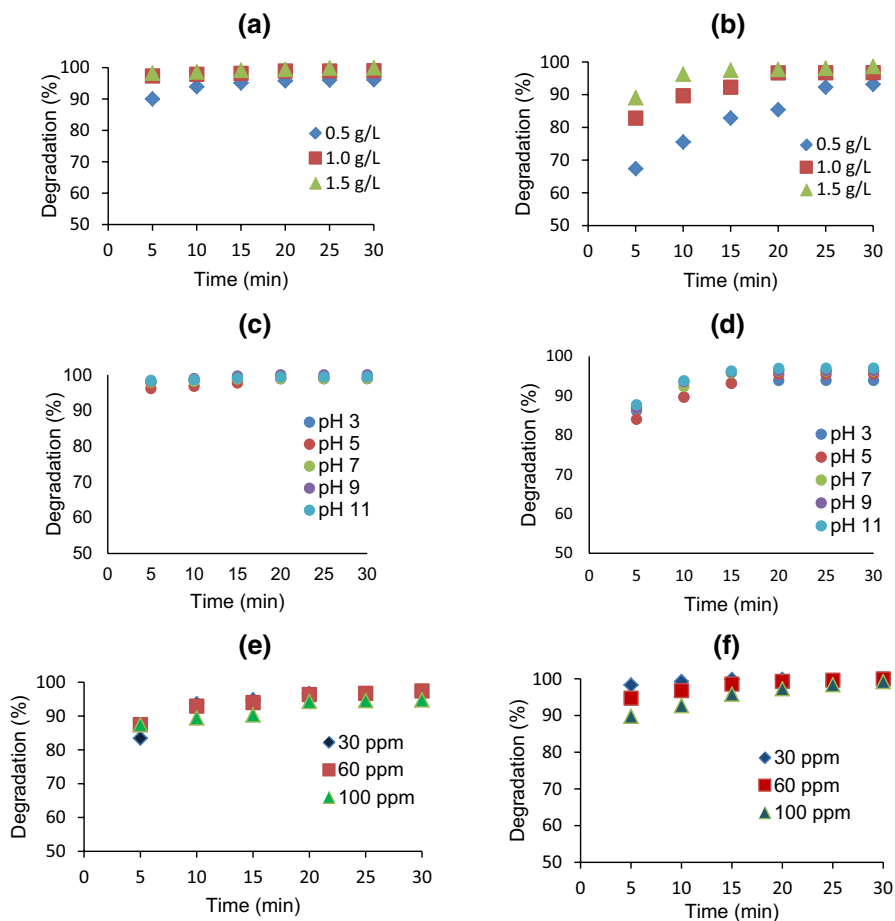
Fig. 5 Effect of catalyst loading on the photodegradation of **a** RO-14 and **b** DR-1 (V = 150 mL, pH 7.0, initial dye conc. = 30.0 mg/L); Effect of pH values on the photodegradation of **c** RO-14 and **d** DR-1(V = 150 mL, catalyst loading = 1 g/L, initial dye conc. = 30 mg/L); Effect of initial dye concentration on the photodegradation of **e** RO-14 and **f** DR-1 (V = 150 mL, pH = 7.0, catalyst loading = 1 g/L)

recombination and the formation of OH^- lead to an increase in pH over time and showed a higher catalytic efficiency [22].

Effect of dye loading

As seen in Fig. 5e and f, increasing the dye concentration from 30 to 100 mg/L decreased the degradation rates and longer times were required to achieve a complete degradation. This observation was supported by the rate constants calculated using the Gabor Lente kinetic model (Table 1). When the concentration of dye was increased, the observed decrease in degradation rates may be due to the unavailability of enough active sites, since the amount of catalyst was kept constant for all

Table 1 The calculated value of rate constant (k), standard deviation (SD) and coefficient of determination (R^2) of RO-14 and DR-1 dyes in different dye concentrations	Dye concentration (mg/L)	RO-14		DR-1	
		k (min^{-1})	R^2	k (min^{-1})	R^2
	30	0.80392	0.99996	0.40888	0.99976
		SD: 0.04322		SD: 0.01454	
	60	0.61986	0.99931	0.47997	0.99854
		SD: 0.05303		SD: 0.03820	
	100	0.47233	0.99566	0.52318	0.99591
		SD: 0.04953		SD: 0.06223	

dye concentrations studied. In spite of increasing the dye concentration, keeping the amount of catalyst constant, caused the relative amounts of $O_2^{·-}$ and OH· radicals on the catalyst's surface not to increase. As a result, the production of holes or hydroxyl radicals that can attack pollutants was limited. Therefore, the relative OH· number attaching the compound decreased so the photodegradation efficiency decreased [23, 24].

Kinetic studies

The kinetic experiments were measured against the RO-14 and DR-1 dye degradation and repeated three times with different initial dye concentrations. The degradation rate of RO-14 and DR-1 (Fig. 6), in the presence of CZF@PANI photocatalyst, is calculated using Eq. 2 [25]. This particular model does least-squares fitting to the exponential curve widely used in pseudo-first-order kinetics.

$$C(t) = Xe^{-kt} + E \qquad (2)$$

here C is the concentration of the solution at time t (mg/L); X is the amplitude (mg/L); k is the first-order rate constant (min^{-1}); and E is the endpoint (mg/L). Exponential curves evaluated by integrating the function over time:
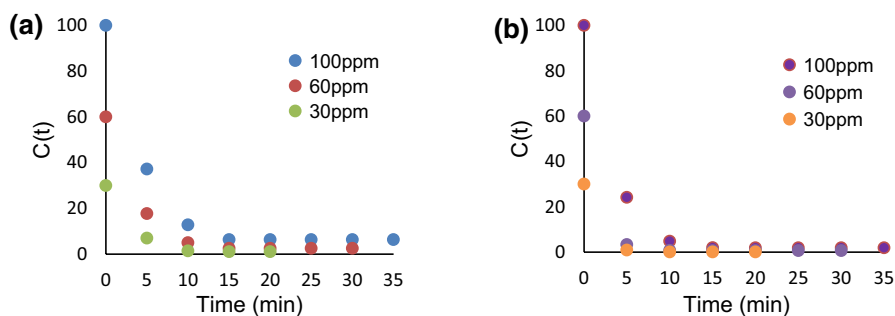

Fig. 6 Degradation kinetics of **a** DR-1 (pH 7.0, CZF@PANI catalyst = 1 g/L, V = 150 mL), and **b** RO-14 (pH 7.0, CZF@PANI catalyst = 1 g/L, V = 150 mL)
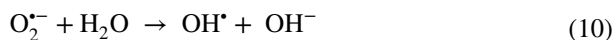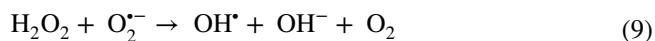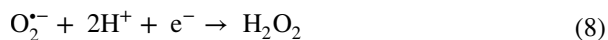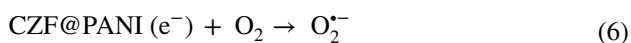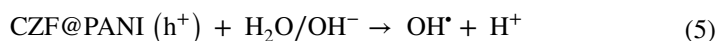
$$C_t^\tau = \frac{1}{\tau}\int_t^{t+\tau}(Xe^{-ks}+E)ds = \frac{1-e^{-k\tau}}{k\tau}Xe^{-kt}+E \tag{3}$$

The first order rate constant (k) value of the prepared catalyst (Table 1) exposed that photocatalytic degradation rate of dye declines with increasing dye concentration within a range of (30 to 100 mg/L) and exhibits a linear relationship with a coefficient of determination ($R^2 > 0.95$).

Proposed mechanism of RO-14 and DR-1 photodegradation

Under visible light irradiation, CZF@PANI composite can produce photogenerated electrons (e^-) and holes (h^+) which can react with H_2O and O_2 to form reactive oxygen species such as hydroxyl free radical ($OH^\bullet$), superoxide anion radical ($O_2^{\bullet-}$) and H_2O_2 [26, 27]. These radicals participate in the oxidative degradation of pollutants on the catalyst's surface. To probe the active species in the degradation process, 5 mL of sodium oxalate (hole scavenger), ethanol ($OH^\bullet$ radicals scavenger), P-benzoquinone ($O_2^{\bullet-}$ scavenger) and silver nitrate (electron scavenger) with a concentration of 0.01 mol/L were separately added to the reaction system for the degradation of RO-14 and DR-1 dyes [28, 29].

This active-species-trapping experiment reveals that, when sodium oxalate and ethanol were added into the photocatalytic system, the degradation efficiency was markedly decreased, suggesting that the holes and hydroxyl radicals served as the main active species in the dye degradation. The degradation rate was moderately inhibited on addition of benzoquinone (BQ), which is a signal that superoxide radicals were responsible for degradation to some extent. Addition of $AgNO_3$ had little or negligible effect on the degradation rate, proving that few electrons were produced and very weakly influenced the rate of degradation. The formation process of active radicals can be explained by the following equations:-

$$CZF@PANI + h\upsilon \rightarrow CZF@PANI\left(e^- + h^+\right) \tag{4}$$

$$CZF@PANI\left(h^+\right) + H_2O/OH^- \rightarrow OH^\bullet + H^+ \tag{5}$$

$$CZF@PANI\left(e^-\right) + O_2 \rightarrow O_2^{\bullet-} \tag{6}$$

$$O_2^{\bullet-} + H^+ \rightarrow HO_2^\bullet \tag{7}$$

$$O_2^{\bullet-} + 2H^+ + e^- \rightarrow H_2O_2 \tag{8}$$

$$H_2O_2 + O_2^{\bullet-} \rightarrow OH^\bullet + OH^- + O_2 \tag{9}$$

$$O_2^{\bullet-} + H_2O \rightarrow OH^\bullet + OH^- \tag{10}$$

$$O_2^{\bullet-};\ HO_2^{\bullet},\ OH^{\bullet},\ h^+ +\ RO-14\ and\ DR-1\ Dye\ \rightarrow\ Degraded\ products \quad (11)$$

The PANI shell can enhance the adsorption of pollutants from solution, and increase the utilization ratio of visible light. Photogenerated holes at HOMO of PANI, including those from VB of CZF, can directly destroy the adsorbed pollutants or react with H_2O (or hydroxide anions) to yield $OH^{\bullet}$ radicals. Due to the large surface area of the CZF@PANI photocatalyst, the available photogenerated electrons assisted the fast degradation of the dye pollutants of wastewater. The photogenerated electrons on CB of CZF, including those from LUMO of PANI, can be captured by dissolved O_2 to yield: (i) the superoxide radical anion, $O_2^{\bullet-}$, (ii) the $HO_2^{\bullet}$ radical upon protonation, and (iii) the $OH^{\bullet}$ radical via trapping electron [30]. The active oxygen species $O_2^{\bullet-}$, $HO_2^{\bullet}$ and $OH^{\bullet}$ radicals, and h^+ have been involved in the degradation of polluted compounds.

CZF@PANI composite for MO, DY-142 and RNB dyes degradation

Further, photocatalytic activity of CZF@PANI composite was evaluated with three more model pollutants: MO, DY-142 and RNB dyes (30 mg/L) under visible light irradiation (Fig. 7). The complete-degradation times for MO, DY-142 and RNB were observed as 15, 30 and 35 min. The results indicate that the photodegradation of MO, DY-142 and RNB by CZF@PANI composite is also much faster than that of other commercial photocatalysts (Table 2). The photocatalytic efficiency of CZF@PANI composite toward MO was obviously higher than it was toward DY-142 and RNB. This difference in efficiency might be attributed to the effect of π–π* stacking, electrostatic attraction, and repulsion [31].

The photocatalytic performances of some PANI-modified heterojunction catalysts have already been reported earlier in Table 2. Based on the photodegradation, degradation time and cyclic stability, the as-synthesized CZF@PANI composite showed the best photocatalytic performance.

Fig. 7 Photocatalytic degradation of MO, DY-142 and RNB in the presence of CZF@PANI composite (dye loading = 30 mg/L, catalyst loading = 1 g/L, pH 7.0)
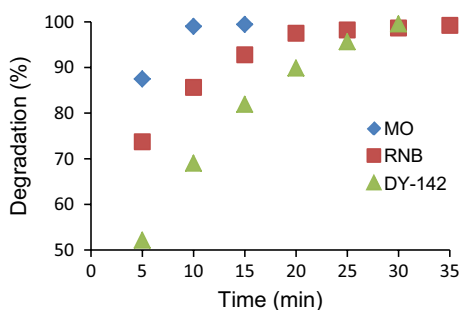
Table 2 Photocatalytic performance of other polyaniline (PANI) coated nanocomposites

Photocatalyst	Irradiation source	Dye conc (mg/L)	Catalyst dose (g/L)	Degradation time (min)	Photo degradation (%)	Cyclic stability, runs/efficiency (%)	Ref
Ag_2CO_3/PANI	Visible	MB (50)	1	90	~ 85.75	4 runs/ ~ 72.8	[32]
$BiYTi_2O_7$/PANI	Visible	AG (20)	2	330	~ 100	4 runs/ ~ 92.5	[33]
PANI/MS-TiO_2	Xenon	MB (10)	1	150	~ 99.5	5 runs / ~ 90	[34]
Fe_3O_4/PANI	Ultra-sound	MO (20)	0.34	180	~ 97.9	5 runs/ ~ 37.3	[35]
$ZnFe_2O_4$/TiO_2/PANI	UV	RhB (5)	0.25	240	~ 98	4 runs/ ~ 88.5	[36]
$CoFe_2O_4$/PANI	Mercury	MO (20)	0.25	540	~ 80	3 runs (not mentioned)	[29]
$Co_{0.5}Zn_{0.5}Fe_2O_4$@PANI	Visible	RO-14 (30)	1	20	~ 99	25 runs/ ~ 88	This study

Photodegradation and evaluation of COD, BOD$_5$ and pH values of real textile dyeing wastewater samples

In order to investigate the capacity of CZF@PANI as a photocatalyst in real textile dyeing wastewater, a set of experiments were conducted on textile wastewater (three different wastewater samples collected with an interval of one day between each two, from Square Fashions Ltd., Bangladesh) containing various persistent organics and color compounds. In all experiments, 0.3 g of CZF@PANI was suspended in 150 mL of the real textile dyeing wastewater, which was placed in a reactor. The decolourization efficiencies differ in wastewater samples because of different types of dyes used in the textile industry. Under optimal conditions, the extent of decolourization of Wastewater-1 was nearly 99% after 50 min, Wastewater-2 was nearly 98% after 60 min, and Wastewater-3 was nearly 98% after 35 min of irradiation. Table 3 indicates the characteristics of real textile dyeing wastewater before and after the treatment by photocatalyst.

The initial (COD) values of three untreated wastewater samples were 260.48, 272.32 and 284.16 mg/L (Table 3). High total reductions of COD concentration were detected for all investigation, after treatment with CZF@PANI. The COD values were reduced to 71.04, 47.36 and 94.72 mg/L. The percentage removal of COD for the wastewater samples ranged from 66 to 82%, indicating great potential of CZF@PANI in industrial wastewater treatment. The COD removal efficiency was calculated using the following equation:

$$\eta = \frac{COD_i - COD_t}{COD_i} \times 100 \tag{12}$$

here η, COD_i and COD_t are removal efficiency, initial chemical oxygen demand, and chemical oxygen demand at time t.

The BOD values of the three untreated wastewater samples were 51.2, 51.2 and 54.4 mg/L. After photocatalytic treatment, the BOD values were reduced to 27.2, 25.6 and 28.48 mg/L. Dissolved oxygen (DO) is essential for the survival of the living organisms, DO is reduced when wastewater containing high BOD values pollutes the local water reservoir. Aerobic bacteria utilise the available DO of water to perform their metabolic activities at higher BOD values. If BOD is excessive, there will be a drastic deficiency of DO and the water will become anaerobic, thus incapable of supporting life.

Table 3 Physicochemical characteristic levels of untreated and treated textile dyeing wastewater

Sample	COD (mg/L)		BOD$_5$ (mg/L)		pH		BSR standard
	Untreated	Treated	Untreated	Treated	Untreated	Treated	
Wastewater-1	260.48	71.04	51.20	27.20	7.64	6.27	pH 6–9
Wastewater-2	272.32	47.36	51.20	25.60	7.58	6.36	COD < 200
Wastewater-3	284.16	94.72	54.40	28.48	7.66	6.80	BOD$_5$ < 30

BSR Business for social responsibility

The pH of untreated real textile dyeing wastewater samples appeared to lay between 7.58 and 7.66. After treatment, the pH of all wastewater was reduced to 6.27–6.80.

Photodegradation of real tannery wastewater

To evaluate the catalytic efficiency of CZF@PANI catalyst on real tannery wastewater under visible light irradiation the discolouration content was measured as a function of time. At first, 150 ml of tannery wastewater, without any pH adjustment, were photo-catalytically treated with the CZF@PANI catalyst (0.3 g) in a reactor, which was directly exposed to light. The complete discolouration of tannery wastewater was obtained after 60 min of irradiation, due to the simultaneous removal of dyes and organic substances in the wastewater. The photocatalytic activity of the prepared catalyst varied in the same order compared to the degradation of synthetic dye wastewater. The degradation rate of real wastewater samples was slower than that of the above-mentioned azo dyes due to the presence of mixtures of organic compounds.

Magnetic separation and recycling (with and without regeneration) performances

The stability of composite was tested in continuous operation during up to 25 cycles under optimised reaction conditions (1 g/L CZF@PANI, initial pH 7, 30 mg/L RO-14) for the oxidative degradation of RO-14. For the recyclability runs, the photocatalyst was separated magnetically, and the degraded RO-14 supernatant was removed. A fresh RO-14 solution were added into it, without washing the used photocatalyst. The photodegradation efficiency was nearly the same as earlier (~ 99%). This procedure was repeated several times. As shown in Fig. 8, about 88% photodegradation efficiencies of RO-14 were achieved even after 25 cycles. Thus the photocatalyst is highly stable during the photocatalytic
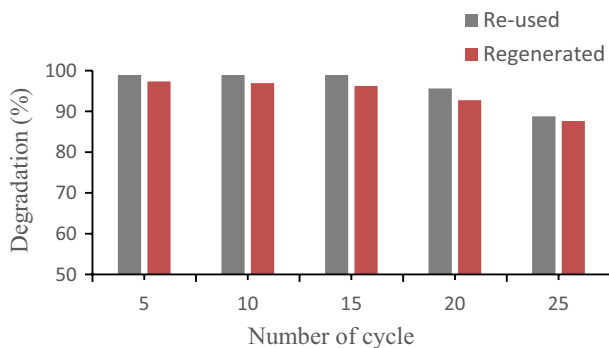

Fig. 8 Dye degradation efficiency of re-used and regenerated (after chemical treatment) CZF@PANI photocatalyst on RO-14 solution (1 g/L CZF@PANI, pH 7.0 and 30 mg/L RO-14, V = 150 mL)

degradation of these organic pollutant molecules. The spinel structure of CZF might have played an important role in this excellent stability and activity of the composite as a synthesized photocatalyst. In addition, the Brunauer, Emmett, and Teller (BET) experimental data of the CZF@PANI photocatalyst exhibited a greater number of reaction sites may also be responsible for fixing more dyes from wastewater.

During application in treatment, the active sites of CZF@PANI are loaded with contaminants or their degradation products are coupled with the loss of important functional groups. To activate the reversible doping-dedoping chemistry of PANI, the regeneration of CZF@PANI was achieved by using NaOH solution (0.1 M) as a desorption agent and HCl solution (1.0 M) as an activation agent. After 25 cycles of re-use, the catalyst, 0.1 M NaOH solution, was used to treat CZF@PANI for 10 min keeping the temperature above 60℃. Then 1.0 M HCl solution was used to treat the CZF@PANI for 60 min to get back to the original semi-conducting state. The regenerated catalyst was washed with water and ethanol. Finally, it was dried in an oven for further use. Repeatedly, the regenerated catalyst was utilised to treat the same concentration of RO-14 solution, and its regeneration stability was studied. Fig. 8 shows the regeneration efficiency of CZF@PANI for degradation of RO-14 solution (30 mg/L). This catalyst's capacity for regeneration and reuse, with the nearly same decolourization efficiency, is an outstanding advantage of the catalyst for wastewater treatment. These capacities reduce the cost of operation and have less impact on the environment than use of other catalysts.

Conclusion

The physico-chemical nature of the CZF@PANI composite indicates that the spinel-structured CZF nanoparticle was well intercalated on the polyaniline matrix. The composite exhibited excellent photocatalytic activity in the degradation of synthetic dyes and real wastewater under visible light irradiation. The synthesised composite is also re-usable and stable in the water environment, as demonstrated by several discolouration tests. Due to the magnetic properties of CZF nanoparticles, the composite can be easily separated by an external magnetic field from an aqueous suspension. The greater surface area of the CZF@PANI reveals the production of a large number of active electrons to degrade the dye contaminants and high efficiencies of RO-14 were achieved even after 25 cycles of photodegradation. The high degradation capability and stability, reusability, and easy separability of the composite make it quite advantageous and also more cost-effective compared to existing traditional photocatalysts. Also, the percentage removal of BOD and COD indicates the great potential of CZF@PANI for the treatment of dye-polluted wastewater.

Declarations

Conflict of interest The authors declare no conflict of interest.

References

1. Punzi M, Nilsson F, Anbalagan A et al (2015) Combined anaerobic-ozonation process for treatment of textile wastewater: removal of acute toxicity and mutagenicity. J Hazard Mater 292:52–60. https://doi.org/10.1016/j.jhazmat.2015.03.018
2. Aich A, Goswami AR, Roy US, Mukhopadhyay SK (2015) Ecotoxicological assessment of tannery effluent using guppy fish (Poecilia reticulata) as an experimental model: a biomarker study. J Toxicol Environ Heal Part A Curr Issues 78:278–286. https://doi.org/10.1080/15287394.2014.960045
3. Gao Y, Fang P, Chen F et al (2013) Enhancement of stability of N-doped TiO_2 photocatalysts with Ag loading. Appl Surf Sci 265:796–801. https://doi.org/10.1016/j.apsusc.2012.11.114
4. Dumrongrojthanath P, Thongtem T, Phuruangrat A, Thongtem S (2013) Synthesis and characterization of hierarchical multilayered flower-like assemblies of Ag doped Bi_2WO_6 and their photocatalytic activities. Superlattices Microstruct 64:196–203. https://doi.org/10.1016/j.spmi.2013.09.028
5. Sackmann EK, Fulton AL, Beebe DJ (2014) The present and future role of microfluidics in biomedical research. Nature 507:181–189
6. Phuruangrat A, Maneechote A, Dumrongrojthanath P et al (2015) Effect of pH on visible-light-driven Bi_2WO_6 nanostructured catalyst synthesized by hydrothermal method. Superlatt Microstruct 78:106–115. https://doi.org/10.1016/j.spmi.2014.11.038
7. Mohammadzadeh Kakhki R, Khorrampoor A, Rabbani M, Ahsani F (2017) Visible light photocatalytic degradation of textile waste water by Co doped $NiFe_2O_4$ nanocomposite. J Mater Sci Mater Electron 28:4095–4101. https://doi.org/10.1007/s10854-016-6028-6
8. Zhang ZJ, Wang ZL, Chakoumakos BC, Yin JS (1998) Temperature dependence of cation distribution and oxidation state in magnetic Mn-Fe ferrite nanocrystals. J Am Chem Soc 120:1800–1804. https://doi.org/10.1021/ja973085l
9. Dhand C, Das M, Datta M, Malhotra BD (2011) Recent advances in polyaniline based biosensors. Biosens Bioelectron 26:2811–2821
10. Yasuhiko S, Kageyama H (2007) Charge carrier transporting molecular materials and their applications in devices. Chem Rev 107:953–1010. https://doi.org/10.1021/cr050143+
11. Dallas P, Stamopoulos D, Boukos N et al (2007) Characterization, magnetic and transport properties of polyaniline synthesized through interfacial polymerization. Polymer (Guildf) 48:3162–3169. https://doi.org/10.1016/j.polymer.2007.03.055
12. Ladgaonkar BP, Kolekar CB, Vaingankar AS (2002) Infrared absorption spectroscopic study of Nd^{3+} substituted Zn-Mg ferrites. Bull Mater Sci 25:351–354. https://doi.org/10.1007/BF02704131
13. Pant A, Tanwar R, Kaur B, Mandal UK (2018) A magnetically recyclable photocatalyst with commendable dye degradation activity at ambient conditions. Sci Rep. https://doi.org/10.1038/s41598-018-32911-3
14. Stejskal J, Sapurina I, Trchová M et al (2006) The genesis of polyaniline nanotubes. Polymer (Guildf) 47:8253–8262. https://doi.org/10.1016/j.polymer.2006.10.007
15. Gu H, Eskizeybek V, Haspulat B et al (2013) Preparation of a new polyaniline / CdO nanocomposite and investigation of its photocatalytic activity : comparative study under UV light and natural sunlight irradiation. Ind Eng Chem Res 52:10924–10934. https://doi.org/10.1021/ie401389e
16. Qian HS, Hu Y, Li ZQ et al (2010) $ZnO/ZnFe_2O_4$ magnetic fluorescent bifunctional hollow nanospheres: Synthesis, characterization, and their optical/magnetic properties. J Phys Chem C 114:17455–17459. https://doi.org/10.1021/jp105583b
17. Borhan AI, Hulea V, Iordan AR, Palamaru MN (2014) Cr^{3+} and Al^{3+} co-substituted zinc ferrite: structural analysis, magnetic and electrical properties. Polyhedron 70:110–118. https://doi.org/10.1016/j.poly.2013.12.022
18. Ao W, Li J, Yang H et al (2006) Mechanochemical synthesis of zinc oxide nanocrystalline. Powder Technol 168:148–151. https://doi.org/10.1016/j.powtec.2006.07.014
19. Debnath S, Ballav N, Nyoni H et al (2015) Optimization and mechanism elucidation of the catalytic photo-degradation of the dyes Eosin Yellow (EY) and Naphthol blue black (NBB) by a

polyaniline-coated titanium dioxide nanocomposite. Appl Catal B Environ 163:330–342. https://doi.org/10.1016/j.apcatb.2014.08.011

20. Cho IH, Zoh KD (2007) Photocatalytic degradation of azo dye (Reactive Red 120) in TiO_2/UV system: Optimization and modeling using a response surface methodology (RSM) based on the central composite design. Dye Pigment 75:533–543. https://doi.org/10.1016/j.dyepig.2006.06.041

21. Siong LL (2016) Photocatalytic degradation of sunset yellow dye over zinc oxide nanoparticles under fluorescent light irradiation. Unpublished Master Thesis, University Tunku Abdul Rahman, Kampar

22. Liu F, Xie Y, Yu C et al (2015) Novel hybrid Sr-doped TiO_2/magnetic $Ni_{0.6}Zn_{0.4}Fe_2O_4$ for enhanced separation and photodegradation of organics under visible light. RSC Adv 5:24056–24063. https://doi.org/10.1039/C5RA00187K

23. El-Bahy ZM, Ismail AA, Mohamed RM (2009) Enhancement of titania by doping rare earth for photodegradation of organic dye (Direct Blue). J Hazard Mater 166:138–143. https://doi.org/10.1016/j.jhazmat.2008.11.022

24. Byrappa K, Subramani AK, Ananda S et al (2006) Photocatalytic degradation of rhodamine B dye using hydrothermally synthesized ZnO. Bull Mater Sci 29:433–438. https://doi.org/10.1007/BF02914073

25. Lente G (2015) Solving Rate Equations. Deterministic kinetics in chemistry and systems biology: the dynamics of complex reaction networks. Springer, Debrecen, pp 21–59

26. Appierot G, Lipovsky A, Dror R et al (2009) Enhanced antibacterial activity of nanocrystalline ZnO due to increased ROS-mediated cell injury. Adv Funct Mater 19:842–852. https://doi.org/10.1002/adfm.200801081

27. Niu J, Yao B, Chen Y et al (2013) Enhanced photocatalytic activity of nitrogen doped TiO_2 photocatalysts sensitized by metallo Co, Ni-porphyrins. Appl Surf Sci 271:39–44. https://doi.org/10.1016/j.apsusc.2012.12.175

28. Xiong P, Wang L, Sun X et al (2013) Ternary titania-cobalt ferrite-polyaniline nanocomposite: a magnetically recyclable hybrid for adsorption and photodegradation of dyes under visible light. Ind Eng Chem Res 52:10105–10113. https://doi.org/10.1021/ie400739e

29. Xiong P, Chen Q, He M et al (2012) Cobalt ferrite-polyaniline heteroarchitecture: a magnetically recyclable photocatalyst with highly enhanced performances. J Mater Chem 22:17485–17493. https://doi.org/10.1039/C2JM31522J

30. Wu T, Liu G, Zhao J et al (1998) Photoassisted degradation of dye pollutants. V. Self-photosensitized oxidative transformation of Rhodamine B under visible light irradiation in aqueous TiO_2 dispersions. J Phys Chem B 102:5845–5851. https://doi.org/10.1021/jp980922c

31. Fu J, Chen Z, Wang M et al (2015) Adsorption of methylene blue by a high-efficiency adsorbent (polydopamine microspheres): kinetics, isotherm, thermodynamics and mechanism analysis. Chem Eng J 259:53–61. https://doi.org/10.1016/j.cej.2014.07.101

32. Asadollahi A, Sohrabnezhad S, Ansari R, Zanjanchi MA (2018) p-n heterojuction in organic (polyaniline)-inorganic (Ag_2CO_3) polymer-based heterojuction photocatalyst. Mater Sci Semicond Process 87:119–125. https://doi.org/10.1016/j.mssp.2018.04.044

33. Luan J, Shen Y, Wang S, Guo N (2017) Synthesis, property characterization and photocatalytic activity of the polyaniline/$BiYTi_2O_7$ polymer composite. Polymers (Basel). https://doi.org/10.3390/polym9030069

34. Deng Y, Tang L, Zeng G et al (2016) Enhanced visible light photocatalytic performance of polyaniline modified mesoporous single crystal TiO_2 microsphere. Appl Surf Sci 387:882–893. https://doi.org/10.1016/j.apsusc.2016.07.026

35. Wang Y, Gai L, Ma W et al (2015) Ultrasound-assisted catalytic degradation of methyl orange with Fe_3O_4/polyaniline in near neutral solution. Ind Eng Chem Res 54:2279–2289. https://doi.org/10.1021/ie504242k

36. Li J, Xiao Q, Li L et al (2015) Novel ternary composites: preparation, performance and application of $ZnFe_2O_4$/TiO_2/polyaniline. Appl Surf Sci 331:108–114. https://doi.org/10.1016/j.apsusc.2015.01.001

Publisher's Note Springer Nature remains neutral with regard to jurisdictional claims in published maps and institutional affiliations.